ACS APPLIED MATERIALS & INTERFACES

Research Article

Cite This: ACS Appl. Mater. Interfaces 2019, 11, 27343−27352

www.acsami.org

Triggering White-Light Emission in a 2D Imine Covalent Organic Framework Through Lanthanide Augmentation

Chidharth Krishnaraj,[†] Anna M. Kaczmarek,[‡] Himanshu Sekhar Jena,[†] Karen Leus,[†] Nicolas Chaoui,[§] Johannes Schmidt,[§] Rik Van Deun,*[,‡] and Pascal Van Der Voort*[,†]

[†]COMOC—Center for Ordered Materials, Organometallics and Catalysis, Department of Chemistry and [‡]L3—Luminescent Lanthanide Lab, Department of Chemistry, Ghent University, Krijgslaan 281-S3, 9000 Ghent, Belgium

[§]Institut für Chemie—Funktionsmaterialien, Technische Universität Berlin, Hardenbergstraße 40, 10623 Berlin, Germany

Supporting Information

ABSTRACT: Recently, covalent organic frameworks (COFs) have emerged as an interesting class of porous materials, featuring tunable porosity and fluorescence properties based on reticular construction principles. Some COFs display highly emissive monocolored luminescence, but attaining white-light emission from COFs is difficult as it must account for a wide wavelength range. White-light emission is highly desired for solid-state lighting applications, and obtaining it usually demands the combination of red-, green-, and blue-light components. Hence, to achieve the targeted white-light emission, we report for the first time grafting of lanthanides (Eu^{3+}/Tb^{3+}) on a two-dimensional imine COF (TTA-DFP-COF). We studied the luminescence properties of the hybrid materials prepared by anchoring Eu^{3+} (red light) and Tb^{3+} (green light) β-diketonate complexes onto the TTA-DFP-COF. Reticular construction is exploited to design strong coordination of Eu^{3+} and Tb^{3+} ions into nitrogen-rich pockets of the imine COF. Mixed Eu^{3+}/Tb^{3+} materials are then prepared to incorporate red and green components along with the inherent blue light from the organic moieties of the COF to produce white-light emission. We show that COFs have the potential for hosting Eu^{3+} and Tb^{3+} complexes, which can be tuned to obtain desired excitations for applications in the field of optoelectronics, microscopy, optical sensing, and bioassay.

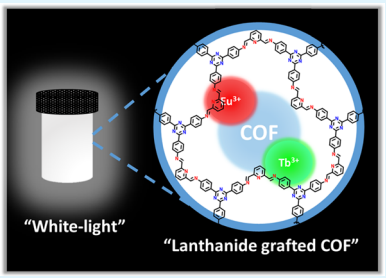

KEYWORDS: *covalent organic framework, reticular chemistry, imine, coordination, luminescence, white-light emission, lanthanide*

INTRODUCTION

Covalent organic frameworks (COFs) are an emerging class of crystalline porous materials,[1] which have shown immense potential for applications in gas adsorption and storage,[2] catalysis,[3,4] batteries,[5,6] and drug delivery.[7,8] Reticular chemistry allows prediction of the crystalline structure by contemplative selection of the molecular building blocks.[9,10] Using these principles, two-dimensional (2D) and three-dimensional COFs have been synthesized using solvothermal methods[11] and under ambient conditions.[12] Several dynamic reversible reactions like imine condensation, boronic ester formation, triazine trimerization, and imide formation have been utilized to create covalent linkages.[1−12] Particularly, imine condensation in which a C═N bond is formed by condensation of an amine ($-NH_2$) with an aldehyde (−CHO) group has been used widely due to easy reaction, stable bond formation, and a wide variety of available monomers. Imine COFs have shown great promise for anchoring metal complexes, which has been employed in metal-based heterogeneous catalysis.[4] Reticular construction principles also allow the design of strong coordination sites on imine COFs, which can be used to achieve strong lanthanide complexation.[13,14]

Recently, COFs have been explored for their luminescence properties. A pyrene- and triphenylene-based boronate COF has been reported that showed blue luminescence occurring purely through the inherent organic components.[15] Also, Crowe et al. synthesized COFs containing a homogeneous and heterogeneous distribution of π-conjugated dehydrobenzoannulene vertex units.[16] These showed bluish green- and yellow-light emission using excitation wavelengths of 350 and 365 nm, respectively. Often, aggregation-caused quenching of $\pi-\pi$ stacked layers occurs due to particle aggregation during COF synthesis.[17] To overcome this, an aggregation-induced emission (AIE) mechanism was introduced, in which AIE columnar arrays were created on COFs. These AIE arrays dominated the luminescence properties and displayed an exceptional quantum yield.[17] Bessinger et al. used larger aromatic groups (isoindigo) as starting monomers to create near-infrared (NIR)-absorbing COFs.[18] The intramolecular donor−acceptor charge delocalization by electron-deficient and electron-rich pairing shifted the absorption into the NIR region. Despite several advancements in COFs, they have

Received: May 4, 2019
Accepted: July 5, 2019
Published: July 5, 2019

DOI: 10.1021/acsami.9b07779
ACS Appl. Mater. Interfaces 2019, 11, 27343−27352

mostly been tuned to emit monocolored lights. Recently, a near-white-light-emitting COF has been constructed by designing a 2D COF with an eclipsed structure and modulating the interlayer and intralayer hydrogen bonding, which allowed access to excited states with different deexcitation pathways. Hence, a dual emission was observed, and by varying the spacer size and side-chain functionalities, near-white photoluminescence (PL) emission was obtained.[19] However, the corresponding Commission internationale de l'éclairage (CIE) coordinates were $x = 0.31$, $y = 0.4$, which are only close to the ideal white-light emission ($x = 0.33$, $y = 0.33$),[20] and also, constructing such COF required intricate designing through complex monomeric units. In addition, Haldar et al.[21] and Ding et al.[22] also reported white-light-emitting COFs with CIE coordinates $x = 0.35$, $y = 0.36$ and $x = 0.30$, $y = 0.35$ respectively. White-light illumination is an important topic of research for solid-state lighting applications.[23−25] A strategy to obtain white light is to have simultaneous emission of red, green, and blue lights,[25] which is not straightforward in COFs, since they contain only organic components. Hence, we implemented a strategy to engineer nitrogen-rich pockets[26] in an imine COF to anchor lanthanides for efficient energy transfer throughout the framework and concurrently provide the extra color augmentation to obtain white-light illumination.

Lanthanide-based luminescence has been studied widely for many years. Particularly, europium and terbium complexes having long luminescence lifetimes have been utilized in the fields of sensors, microscopy, and bioassay.[27,28] Lanthanides grafted onto periodic mesoporous organosilicas (PMOs) have been reported to show luminescence properties in both the visible and NIR regions.[29,30] Also, Ln^{3+} metal−organic frameworks (Ln-MOFs) demonstrate characteristic optical performance because of lanthanide-based luminescence.[31] This occurs from Ln^{3+} components and organic monomers with aromatic/conjugated π-systems.[32] Further, lanthanide complexes were made more thermally stable by anchoring them onto zeolite L material.[33] In addition, several Ln^{3+}/zeolite materials have been reported with focus on improved visible and NIR luminescent sensors.[34] Lanthanide coordination polymers have also been reported to obtain white-light emission.[35,36] However, to the best of our knowledge, lanthanides have not yet been grafted onto COFs.

Herein, we report for the first time lanthanides (Eu^{3+}, Tb^{3+}) coordinated to a 2D imine COF (TTA-DFP COF) showing excellent emission in the red, green, yellow, orange, and white regions. Nitrogen-containing coordination pockets are designed on the TTA-DFP COF by careful selection of monomers.[26] An imine-pyridine ligand containing COF is targeted as (1) they can provide a suitable coordination environment/pocket to accommodate the lanthanide complexes,[37,38] (2) the organic bridging monomer by itself enables excitation of Ln^{3+} through intramolecular energy transfer ("antenna effect"),[39] (3) the porous environment of the COF can be easily grafted with additional ions through a postmodification approach,[14] and (4) the strong coordination sites allow it to be stable to air and moisture.[26,37] For luminescence, we chose to graft Eu^{3+} and Tb^{3+} hexafluoroacetylacetone (hfac) complexes into the pores of the TTA-DFP COF. The β-diketonate ligands have a double function in these materials. First, they shield the first coordination sphere of the Ln^{3+} ion from H_2O molecules, and second, they provide an additional ligand through which the Ln^{3+} ions can be excited. Ligands with C−F groups (such as hfac) instead of C−H groups have been chosen to prevent luminescence quenching. β-Diketonate complexes are well known for their very strong luminescence properties but show several downsides such as low thermal and chemical stabilities as well as poor processability.[40] To overcome this, many researchers propose grafting them into the pores of other materials.[29] We extended this notion to prepare Ln-COFs showing white-light emission by combining red, green, and blue emissions from lanthanides and the organic component of the COF. White-light emission was obtained by grafting the material with different ratios of Eu^{3+} to Tb^{3+} ions and later varying the excitation wavelength. To the best of our knowledge, this is the first example of lanthanide-grafted COFs, and with this report, we introduce a new type of hybrid material based on a 2D COF grafted with β-diketonate complexes for luminescence applications.

EXPERIMENTAL SECTION

Materials. Unless stated otherwise, all reagents were purchased from commercial sources and used without further purification. 4,4′4″-(1,3,5-Triazine-2,4,6-triyl)trianiline (TTA) was synthesized according to a previously reported method[3] (Scheme S1).

Synthesis of TTA-DFP-COF. In a flask, 4,4′4″-(1,3,5-triazine-2,4,6-triyl)trianiline (TTA) (177 mg, 0.5 mmol) was dissolved in a mixture of mesitylene (2 mL) and 1,4-dioxane (3 mL). 2,6-Diformylpyridine (DFP) (101 mg, 0.75 mmol) was weighed separately and dissolved in a mixture of mesitylene (2 mL) and 1,4-dioxane (3 mL). The DFP mixture was then added slowly to the TTA mixture and precipitation was observed. Then, 0.5 mL of 6 M acetic acid was added dropwise and the flask was then kept still for 2 days under ambient conditions. Finally, the precipitate was filtered and washed with distilled water, diethyl ether, tetrahydrofuran, and acetone. After drying the materials at 90 °C for 24 h under vacuum, TTA-DFP COF (230 mg) was obtained as a yellow solid (Scheme S2).

Synthesis of Ln@COFs. In the general procedure, an excess molar amount of the $Ln(hfac)_3(H_2O)_2$ complex (prepared according to a previously reported synthesis)[28] was weighed and dissolved in 5 mL of methanol. In a Pyrex tube, the TTA-DFP COF was weighed, to which the methanol solution of the lanthanide complex was added. The tube was closed with a cap and the suspension was treated with ultrasound for 20 min. Then, it was left for 24 h at room temperature to soak in the lanthanide solution without stirring or heating. Applying this step significantly increased the amount of grafted lanthanide complexes onto the COF support. Afterward, it was placed on a heating block set to 85 °C and heated for 24 h. After cooling down to room temperature, the powder was filtered and washed a few times with methanol to remove any lanthanide ion absorbed on the surface. The powder was dried in an oven at 60 °C (Scheme S3).

Instrumentation. Fourier transform infrared (FT-IR) spectroscopy in the region 4000−650 cm^{-1} was performed with a Thermo Nicolet 6700 FT-IR spectrometer equipped with a nitrogen-cooled MCT detector and a KBr beam splitter. Nitrogen adsorption−desorption isotherms were obtained using a Belsorp Mini apparatus measured at 77 K. Elemental analyses (C, H, N, and O) were carried out on a Thermo Scientific Flash 2000 CHNS-O analyzer equipped with a TCD detector. X-ray powder diffraction patterns were collected on a Thermo Scientific ARL X'Tra diffractometer, operated at 40 kV, 30 mA using Cu Kα radiation ($\lambda = 1.5406$ Å). Thermogravimetric analysis (TGA) was performed on a Neetzsch STA-449 F3 Jupiter-simultaneous TG-DSC analyzer in the temperature range of 20−800 °C, under a N_2 atmosphere and at a heating rate of 2 °C/min. ^{13}C cross-polarization magic-angle spinning (CP/MAS) NMR spectra were acquired at 125.69 MHz using a 4 mm MAS NMR probe with a spinning rate of 8 kHz and a pulse width of 2.5 μs for a $\pi/4$ pulse. A total of 1800−2700 scans were further accumulated with a 4 s recycle delay. X-ray photoelectron spectroscopy (XPS) measurements were performed on a Thermo Fisher Scientific Escalab 250 Xi.

DOI: 10.1021/acsami.9b07779
ACS Appl. Mater. Interfaces 2019, 11, 27343−27352

Scheme 1. Scheme for the Formation of TTA-DFP COF and Grafting of Lanthanide Complexes to Obtain White-Light Emission

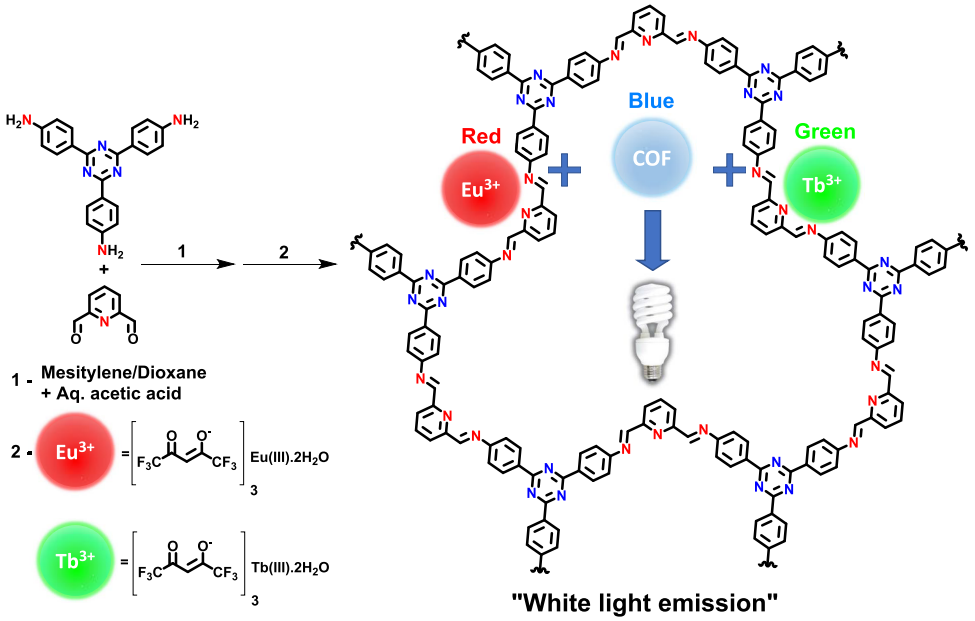

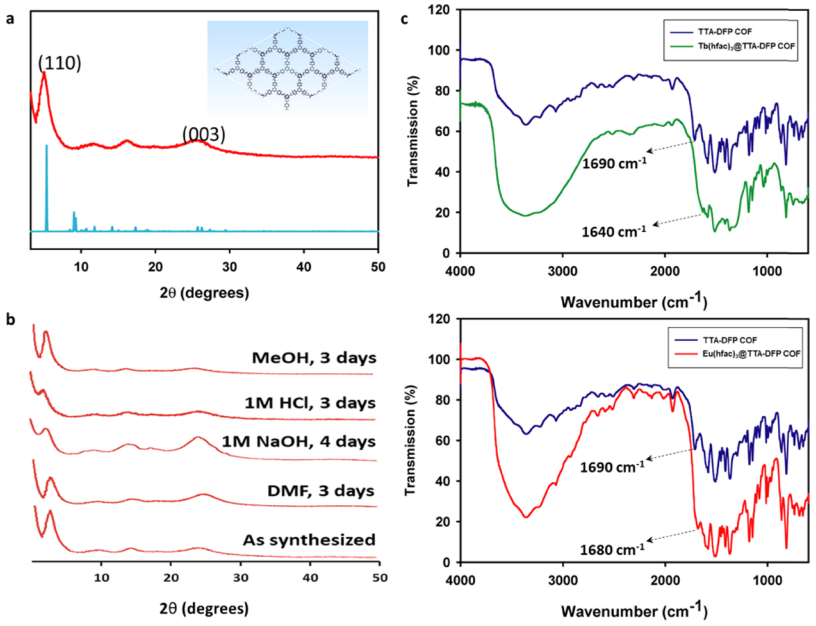

Figure 1. (a) Experimental PXRD pattern of TTA-DFP COF (red) and simulated PXRD pattern of ideal TTA-DFP COF (blue). (b) PXRD patterns of TTA-DFP COF after treatment under different conditions. (c) Diffuse reflectance infrared Fourier transform spectroscopy FT-IR spectra showing the formation of TTA-DFP COF and the shifting of the C═N stretching peak corresponding to successful grafting of Eu^{3+} and Tb^{3+} complexes on TTA-DFP COF.

Luminescence measurements were performed on an Edinburgh Instruments FLSP920 UV−vis−NIR spectrometer setup. A 450 W Xe lamp was used as the steady-state excitation source. Luminescence decay times of the lanthanide samples were recorded using a 60 W pulsed Xe lamp, operating at a frequency of 100 Hz. The photoluminescence (PL) decay kinetic of the ungrafted TTA-DFP COF material was measured using a Supercontinuum white-light laser for time-correlated single photon counting. A Hamamatsu R928P photomultiplier tube was used to detect the emission signals in the near-UV to visible range. Absolute quantum yields were measured by using an integrated sphere with a BENFLEC coating provided by Edinburgh Instruments, as follows

$$\eta = \frac{\int L_{\text{emission}}}{\int E_{\text{blank}} - \int E_{\text{sample}}} \quad (1)$$

where L_{emission} is the integrated value of the emission spectrum, and E_{blank} and E_{sample} are the integrated values of the "excitation" band of the blank and the excitation band of the sample (since the sample absorbs part of the light, this value will be smaller than Eblank), respectively.

To compare the luminescence measurements, all of them have been carried out on the same amounts of powder. Additionally, the same slit size, step, and dwelling time were used for all measurements. For the measurements, solid powdered samples were put between

DOI: 10.1021/acsami.9b07779
ACS Appl. Mater. Interfaces 2019, 11, 27343−27352

quartz plates (Starna cuvettes for powdered samples, type 20/C/Q/0.2). All emission spectra in the manuscript have been corrected for detector response.

RESULTS AND DISCUSSION

TTA-mesitylene/dioxane solutions were prepared and mixed with DFP-mesitylene-dioxane solution to produce TTA-DFP COF (Scheme 1) by an imine condensation reaction. Acetic acid (6 M) was added as an acid catalyst to accelerate the polymerization process. TTA-DFP COF is insoluble in water and in common organic solvents (like tetrahydrofuran, diethyl ether, acetone, methanol, ethanol, *N*,*N*-dimethylformamide, dichloromethane, trichloromethane, dimethyl sulfoxide). The presence of a stretching band at 1690 cm^{-1} in the FT-IR spectra confirms the successful formation of the imine bond (C═N) (Figure 1c). In comparison to the FT-IR spectra of the pristine TTA monomer and DFP monomer, the stretching bands corresponding to the aldehyde (1720−1740 cm^{-1}) and the amine group (3300−3400 cm^{-1}) in the COF are greatly attenuated (Figures S2 and S3), which further implies the successful imine condensation. However, due to the unreacted monomers at the terminal edges of the COFs, residual signals are observed, which has been reported previously for imine COFs.[41] The TTA-DFP COF formation was also verified by solid-state NMR spectroscopy. Figure 2 shows the ^{13}C CP/MAS NMR spectrum of the TTA-DFP COF. The ^{13}C NMR peak at ∼157 ppm corresponds to the characteristic imine carbon atom of the C═N bond.[41] The signals at ∼120, 126, 130, ∼150, and 167 ppm are assigned to the carbon atoms of the phenyl and triazine groups. The minor peaks at 110 and 187 ppm are due to the unreacted terminal monomers in the TTA-DFP COF framework.[41] Based on the geometry of the starting monomers, models were built using distorted hcb layered structures generated in the trigonal *P*3 space group and geometrically optimized with universal force-field energy minimizations.[42] PXRD pattern of the TTA-DFP COF (Figure 1a) shows a crystalline framework formation with an intense peak at $2\theta = 5°$, which is assigned to the (110) plane and corresponds to a *d*-spacing of 17.6 Å. The peak at $2\theta = 25.6°$ is observed due to 2D sheet stacking arising from π-π interactions corresponding to the reflection from the (003) plane (Figure S4 and Tables S1 and S2).[42] The best match was obtained with an ABC sequence, resulting in unit cell parameters of $a = b = 33.0$ Å and $c = 10.39$ Å.[42] The 2D stacking plane distance was 3.5 Å, matching the simulated structure. To further improve the crystallinity of the TTA-DFP COF, several synthesis conditions were tried (Table S3). However, for all of the methods, the corresponding PXRD patterns (Figure S7) were similar and could not be improved further. This can be due to the topology of the aldehyde monomer, which is not linear and is bent. Due to this geometrical restriction, achieving long-range order is difficult under the used synthesis conditions.

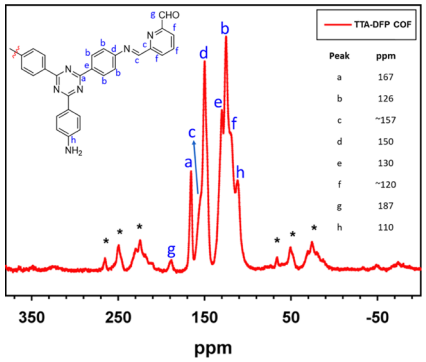

Figure 2. ^{13}C-ss-CP/MAS-NMR spectrum of TTA-DFP COF. g and h correspond to unreacted terminal monomers. * corresponds to the spinning side bands.

Elemental analysis was used to calculate the amount of C, H, and N in the COF. Table S4 shows the elemental content of the TTA-DFP COF and the corresponding theoretical values. The experimental C/N ratio is close to the theoretical value, further providing evidence for the expected formation of the imine-linked COFs. Furthermore, thermogravimetric analysis (TGA) showed that the TTA-DFP COF is thermally stable up to 455 °C (Figure S8). The stability of the TTA-DFP COF under different solvents as well as basic and acidic conditions was tested, and the corresponding PXRD patterns are given in Figure 1b. TTA-DFP COF is stable after treating with methanol (3 days), DMF (3 days), and 1 M NaOH (4 days). However, under acidic conditions (1 M HCl, 3 days), the COF partially loses crystallinity due to hydrolysis of the imine bonds. In the presence of 12 M HCl (within an hour), the TTA-DFP COF is destroyed completely.

The porous properties of the COF were analyzed through nitrogen (N_2) sorption measurements at 77 K. Figure 3 shows a sharp increase in the gas uptake observed at low relative pressure ($P/P_0 < 0.1$) indicating the presence of micropores. A rise in the isotherm at higher relative pressures ($0.8-0.99P/P_0$) occurs due to the presence of textural mesopores caused by agglomeration of the COF crystals.[43] The pore size distribution is shown in Figure S9. The Brunauer−Emmett−Teller (BET) surface area and Langmuir surface area of TTA-DFP COF are 265 and 371 $m^2\ g^{-1}$, respectively.

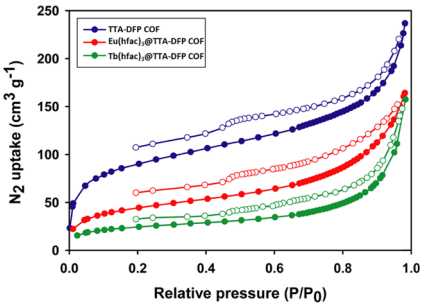

Figure 3. Nitrogen (N_2) sorption isotherms of TTA-DFP COF, Eu(hfac)$_3$@TTA-DFP COF, and Tb(hfac)$_3$@TTA-DFP COF.

Lanthanide complexes were successfully grafted onto the COF through a postmodification approach. The successful grafting of Eu^{3+} and Tb^{3+} complexes on the TTA-DFP COF was observed through FT-IR spectra (Figure 1c), where due to lanthanide coordination, the imine peak shifted from 1690 to 1680 cm^{-1} for Eu(hfac)$_3$@TTA-DFP COF and to 1640 cm^{-1} for Tb(hfac)$_3$@TTA-DFP COF. Due to higher Lewis acidity of terbium, a higher shift is observed in Tb(hfac)$_3$@TTA-DFP COF compared to Tb(hfac)$_3$@TTA-DFP COF. Additionally, the overall N_2 uptake of Eu(hfac)$_3$@TTA-DFP COF and Tb(hfac)$_3$@TTA-DFP COF decreased in comparison to TTA-DFP COF, which corresponds to the presence of lanthanide complexes due to successful grafting on the TTA-DFP COF (Figure 3). Figure S9 shows the pore size distribution of the

DOI: 10.1021/acsami.9b07779
ACS Appl. Mater. Interfaces 2019, 11, 27343−27352

TTA-DFP COF and Ln@TTA-DFP COF samples. The micropores (0.97 nm) are filled when Eu^{3+} and Tb^{3+} complexes are anchored in the COF. ICP-OES analysis showed 2.3 wt % Eu content and 3.1 wt % Tb content in the $Eu(hfac)_3$@TTA-DFP COF and $Tb(hfac)_3$@TTA-DFP COF, respectively. Further, X-ray photoelectron spectroscopy (XPS) analysis was performed for TTA-DFP COF, $Eu(hfac)_3$@TTA-DFP COF, and $Tb(hfac)_3$@TTA-DFP COF. In Figure S10, the observed N 1s peak at binding energy of 397.88 eV can be assigned to the characteristic imine nitrogen peak.[44,45] For the Ln@TTA-DFP COF-samples, this peak is shifted to 399.08 eV. The shift of 1.2 eV binding energy indicates coordination of Eu^{3+} and Tb^{3+} complexes on the TTA-DFP COF. In addition, the oxidation states of the lanthanides were studied through XPS analysis (Figure 4). For

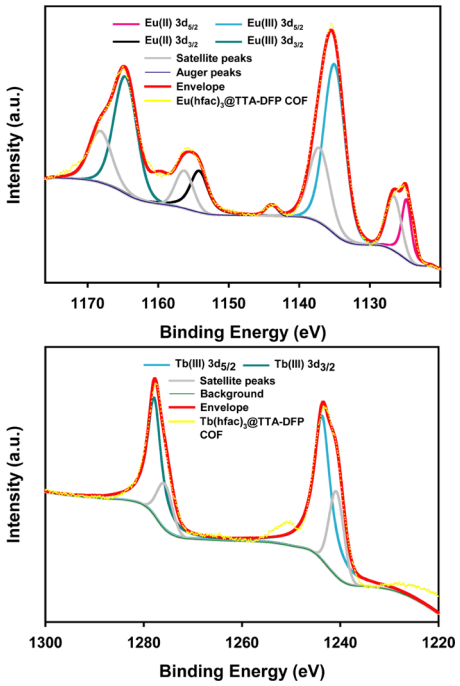

Figure 4. (Top) Deconvoluted XPS images of $Eu(hfac)_3$@TTA-DFP COF; (bottom) deconvoluted XPS images of $Tb(hfac)_3$@TTA-DFP COF.

$Eu(hfac)_3$@ TTA-DFP COF, the characteristic peaks for Eu(III) $3d_{3/2}$ and Eu(III) $3d_{5/2}$ were observed at 1164.66 and 1135 eV, respectively.[46] Also, peaks at 1154.21 and 1124.81 eV appear corresponding to Eu(II) $3d_{3/2}$ and Eu(II) $3d_{5/2}$.[47,48] However, this probably originates from a reduction occurring during the measurement. Furthermore, shakeup satellite peaks are also observed.[46] For $Tb(hfac)_3$@TTA-DFP COF, the characteristic peaks for Tb(III) $3d_{5/2}$ were observed at 1243.78 eV, and for Tb(III) $3d_{3/2}$, they were observed at 1277.98 eV. The difference of ca. 1.9−2.9 eV between the Tb3d and the corresponding satellites has been observed previously.[49] This indicates an oxidation state for Tb of 3+ in our case, as the difference of ∼12 eV binding energy between Tb(III) and Tb(IV) was calculated.[50] The BET surface area and the Langmuir surface area of $Eu(hfac)_3$@TTA-DFP COF decreased to 135 and 197 $m^2\ g^{-1}$, respectively. Similarly, the BET surface area and Langmuir surface area of $Tb(hfac)_3$@TTA-DFP COF decreased to 72 and 110 $m^2\ g^{-1}$, respectively. Furthermore, the decrease in total pore volume of the material from 0.37 to 0.25 $cm^3\ g^{-1}$ and 0.24 $cm^3\ g^{-1}$ for $Eu(hfac)_3$@TTA-DFP COF and $Tb(hfac)_3$@TTA-DFP COF, respectively, shows that the lanthanide complexes are grafted well inside the pores of the COF. In addition, transmission electron microscopy-energy-dispersive X-ray (TEM-EDX) analysis was done to study the distribution of the lanthanide in the material after postmodification through lanthanide grafting (Figures S11 and S12). A homogeneous distribution of Eu and Tb was observed in $Eu(hfac)_3$@TTA-DFP COF and $Tb(hfac)_3$@TTA-DFP COF, respectively.

The combined excitation−emission spectrum of the non-grafted TTA-DFP COF is shown in Figure S14. The maximum of the broad band in the excitation spectrum is located at 370 nm, and the maximum of the emission spectrum is at 439 nm (blue). The decay time of the TTA-DFP COF material was calculated to be 0.76 ns (Figure S15). The Ln@TTA-DFP COF hybrid materials were prepared by grafting TTA-DFP COF with an excess of $Ln(hfac)_3(H_2O)_2$ (Ln = Eu^{3+}, Tb^{3+}) complexes, and further their luminescence properties were investigated. The luminescence spectra and the decay profile of the as-synthesized lanthanide complexes are presented in Figures S16−S19. Figure 5 shows the combined excitation−

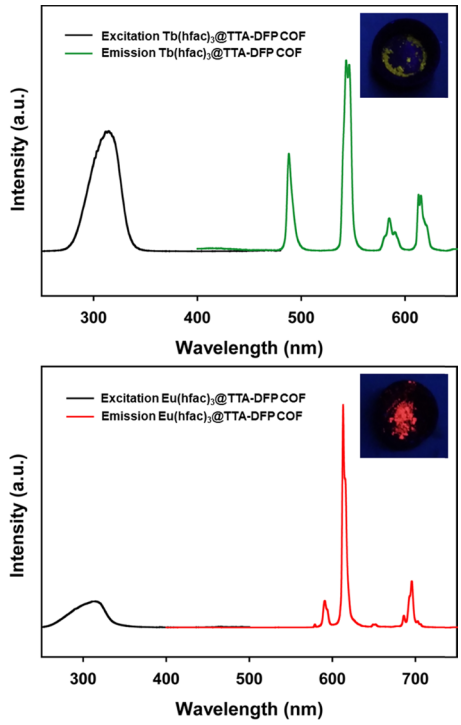

Figure 5. (Top) Combined excitation−emission spectrum of $Eu(hfac)_3$@TTA-DFP COF. The material was excited at 317 nm and observed at 613 nm. (Bottom) Combined excitation−emission spectrum of $Tb(hfac)_3$@TTA-DFP COF. The material was excited at 313 nm and observed at 542 nm.

emission spectra of $Eu(hfac)_3$@TTA-DFP COF and $Tb(hfac)_3$@TTA-DFP COF. In the excitation spectra of both materials, a broad band around 250−340 nm is observed. No f−f transitions are observed in the excitation spectra. When exciting the materials into the maximum of the broad band, the characteristic Eu^{3+} peaks are observed for $Eu(hfac)_3$@TTA-DFP COF and the characteristic peaks of Tb^{3+} are observed for $Tb(hfac)_3$@TTA-DFP COF. The labeled peaks have been assigned to the appropriate transitions in the Supporting

DOI: 10.1021/acsami.9b07779
ACS Appl. Mater. Interfaces 2019, 11, 27343−27352

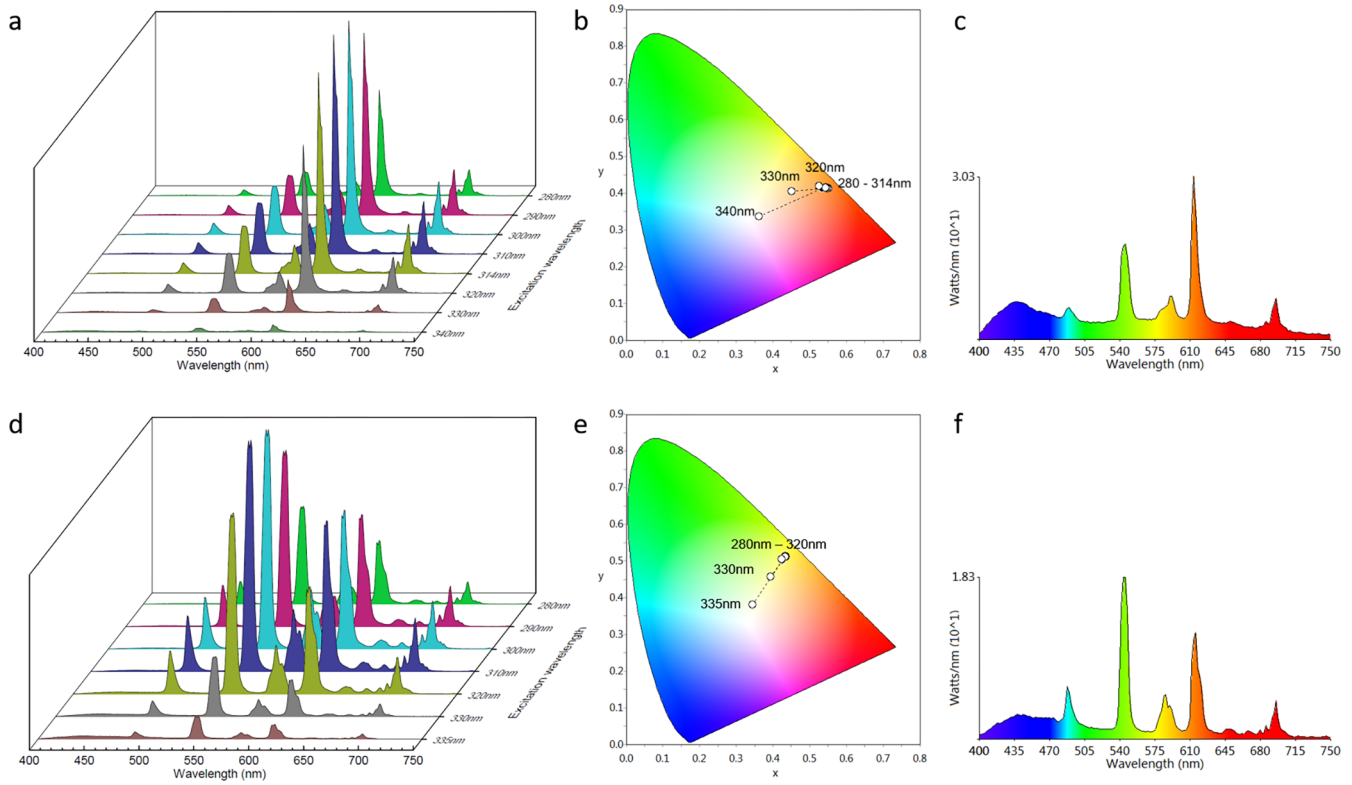

Figure 6. (a) Emission map of 10%Eu,90%Tb@TTA-DFP COF excited at different wavelengths ranging from 280 to 340 nm. (b) CIE coordinate diagram presenting the emitted color by the material when excited at different wavelengths. (c) Emission spectrum with rainbow curve plotted underneath for 10%Eu,90%Tb@TTA-DFP COF material excited at 340 nm. (d) Emission map of 1%Eu,99%Tb@TTA-DFP COF excited at different wavelengths ranging from 280 to 335 nm. (e) CIE coordinate diagram presenting the emitted color by the material when excited at different wavelengths. (f) Emission spectrum with rainbow curve plotted underneath for 1%Eu,99%Tb@TTA-DFP COF material excited at 335 nm.

Information (SI, Tables S5 and S6). The $Eu(hfac)_3$@TTA-DFP COF material yielded red emission, whereas the $Tb(hfac)_3$@TTA-DFP COF material yielded green emission. The corresponding decay profiles are shown in Figures S20 and S21.

To generate white-light emission, several mixed Eu^{3+}/Tb^{3+} materials were prepared, where the ratio of the two ions was varied. Here, we present two of these materials, which resulted in white-light emission. The first material was prepared at a Eu^{3+}/Tb^{3+} ratio of 10:90 (7.2:92.8 based on X-ray fluorescence (XRF) analysis). TEM-EDX analysis shows a homogeneous distribution of Eu and Tb in the TTA-DFP COF after grafting (Figure S13). In this material, several Tb^{3+} ($^5D_4 \rightarrow {}^7F_6$, $^5D_4 \rightarrow {}^7F_5$) and Eu^{3+} ($^5D_0 \rightarrow {}^7F_1$, $^5D_0 \rightarrow {}^7F_2$, $^5D_0 \rightarrow {}^7F_3$, $^5D_0 \rightarrow {}^7F_4$) peaks could be discriminated. When exciting into the maximum of the excitation band (Figures S22–S24 for combined excitation–emission spectra and decay profiles), the observed emission color was orange. By varying the excitation wavelength, we could obtain white-light emission from this material. Figure 6a presents an emission map of 10% Eu,90%Tb@TTA-DFP COF recorded at different excitation wavelengths. Varying the excitation wavelength not only changes the ratio of the Eu/Tb peaks (therefore the ratio of the red to green color), but also when exciting at a longer wavelength, a blue component is observed. The presence of the blue light in the material after grafting the lanthanides could be caused by two factors: (1) incomplete energy transfer from the COF material to the Ln^{3+} ions (Tb^{3+}/Eu^{3+}) and (2) some sites of the COF are not grafted with lanthanide ions. The first case is rather unlikely as we see in the $Eu(hfac)_3$@TTA-DFP COF and $Tb(hfac)_3$@TTA-DFP COF emission spectra (Figure 5) that the energy transfer from the COF material to the lanthanides is very efficient (no broad band present in the spectrum and also no f–f peaks in the excitation spectra). Therefore, the second case is the only possibility, which means that certain sites of the COF are not grafted and emit blue light when excited at varied wavelengths. The excitation wavelength-dependent emission for the $Eu(hfac)_3$@TTA-DFP COF and $Tb(hfac)_3$@TTA-DFP COF shows a broad ligand band in the emission spectrum even when not exciting into the ligand band maxima (Figure S25). This can be assigned to the emission of ungrafted COF sites. It should be mentioned here that grafting COFs with lanthanides is not as straightforward as grafting MOFs. An excess of the lanthanide salt/complex needs to be added to obtain strong luminescence properties of the material. Also, we have proposed a method with a soaking step as we have observed the grafting of the lanthanide ions is then more efficient. As can be seen in Figure S14, the maximum of the original blank TTA-DFP COF is 370 nm. When exciting at higher wavelengths, the nongrafted COF sites are excited more than the grafted sites of the COF (maxima, 313 and 317 nm). The presence of this blue component allows acquiring close to ideal white-light emission. The change of color when varying the excitation wavelength has been visualized on a CIE color diagram presented in Figure 6b. When the material was excited at 340 nm, the calculated CIE coordinates were $x = 0.3636$, $y = 0.3355$ (for a full list of CIE coordinates, see Table S7). In Figure 6c, we present the emission spectrum of 10%Eu,90%

DOI: 10.1021/acsami.9b07779
ACS Appl. Mater. Interfaces 2019, 11, 27343–27352

Table 1. Luminescence Decay Times of the Lanthanide Materials

sample	τ_1 (μs)	τ_2 (μs)	τ_{av} (μs)
$Eu(hfac)_3(H_2O)_2$	703.9		703.9
$Tb(hfac)_3(H_2O)_2$	311.2		311.2
$Eu(hfac)_3$@TTA-DFP COF	125.6 (19%)	468.1 (81%)	447.8
$Tb(hfac)_3$@TTA-DFP COF	217.9 (50%)	1096.7 (50%)	951.3
10%Eu,90%Tb@TTA-DFP COF obs Eu	585.2		585.2
10%Eu,90%Tb@TTA-DFP COF obs Tb	32.6 (96%)	201.4 (4%)	63.1
1%Eu,99%Tb@TTA-DFP COF obs Eu	950.7		950.7
1%Eu,99%Tb@TTA-DFP COF obs Tb	131.2 (77%)	889.0 (33%)	639.4

Tb@TTA-DFP COF upon 340 nm excitation with a rainbow fitted underneath the curve to visualize the different color components. The obtained quantum yield was 3.1%. In addition, we present the results for the second material, prepared at a Eu^{3+}/Tb^{3+} ratio of 1:99 (1.8:98.2 based on XRF analysis). Also, in the emission spectrum of this material, the Tb^{3+} ($^5D_4 \rightarrow {}^7F_6$, $^5D_4 \rightarrow {}^7F_5$) and Eu^{3+} ($^5D_0 \rightarrow {}^7F_1$, $^5D_0 \rightarrow {}^7F_2$, $^5D_0 \rightarrow {}^7F_3$, $^5D_0 \rightarrow {}^7F_4$) peaks are visible (Figure S26). When exciting into the maximum of the excitation peak, yellow emission light is obtained. In this case, by changing the excitation wavelength to 335 nm, a warm white-light emission can be obtained ($x = 0.3442$, $y = 0.3801$). The corresponding emission map, CIE color diagram (for a full list of CIE coordinates, see Table S8), and emission spectrum with a rainbow fitted underneath the curve of 1%Eu,99%Tb@TTA-DFP COF are given in Figure 6d–f. The obtained quantum yield was 2.8%. It should be mentioned here that the very precise determination of the lanthanide grafting amount is very important for the reproducibility of these results. It can be seen that the amount of the lanthanide complexes (and ratio between the lanthanides) is not identical to what was used in the synthesis.

To analyze the potential energy transfer from Tb^{3+} to Eu^{3+} in the mixed materials, we have measured the decay times for all samples. All results are presented in Table 1, and decay profiles are presented in the SI (Figures S27 and S28). The average decay times were calculated using eq S1. The decay times clearly indicate that there is an energy transfer present between the Tb^{3+} and Eu^{3+} ions in the mixed Eu,Tb@TTA-DFP COF materials. In these materials, the decay time of Tb^{3+} decreases compared to $Tb(hfac)_3$@TTA-DFP COF, whereas the decay time of Eu^{3+} significantly increases compared to $Eu(hfac)_3$@TTA-DFP COF, indicating an efficient energy transfer between the two ions. Another interesting observation that can be made based on the luminescence decay times is the significant increase of the decay time in $Tb(hfac)_3$@TTA-DFP COF material compared to the pure $Tb(hfac)_3(H_2O)_2$ complex. The opposite trend is observed for the $Eu(hfac)_3$@TTA-DFP COF material. This can most likely be linked to the position of the triplet level of the TTA-DFP COF suggesting that it is more favorable for Tb^{3+} ions. To investigate this, we have prepared and measured a Gd@TTA-DFP COF compound at 77 K in an ethanol/methanol solution (Figures S29 and S30). The triplet level was determined to be around 23 753 cm^{-1}. Therefore, with this measurement, we confirm that the COF triplet level is more favorable for Tb^{3+} as it is located closer to the $^5D_4$ accepting level of Tb^{3+} than to the Eu^{3+} accepting levels.

We have calculated the efficiency of the energy transfer between the Tb^{3+} and Eu^{3+} in the mixed materials based on the luminescence decay times. It is known that from the emission intensity of the sensitizer, the energy transfer efficiency (η_{ET}) from the sensitizer to an activator can be obtained using the following equation

$$\eta_{ET} = 1 - \frac{I_s}{I_{s0}} \tag{2}$$

where I_{s0} is the intrinsic luminescence intensity of Tb^{3+} and I_s is the luminescence intensity of Tb^{3+} in the presence of Eu^{3+}.[51,52] For the 1%Eu,99%Tb@TTA-DFP COF, the efficiency was calculated to be 32.8%. For the 10%Eu,99% Tb@TTA-DFP COF, it was calculated to be 93.4%. We observe that the efficiency of the energy transfer increases with the increase of Eu^{3+} concentration meaning that the energy transfer from Tb^{3+} to Eu^{3+} is very efficient. It is known that the distance between the donor and acceptor determines the energy transfer. To verify the mechanism of energy transfer, Dexter's formula of multipolar interaction and Reisfeld's approximation can be used as follows

$$\frac{I_{s0}}{I_s} \propto C^{n/3} \tag{3}$$

where C is the Eu^{3+} concentration, I_s is the luminescent intensity of Tb^{3+} in mixed Tb,Eu material, and I_{s0} is the intrinsic luminescent intensity of the pure Tb material.[53] Based on this equation, $n = 6$, 8, and 10 correspond to dipole–dipole, dipole–quadrupole, and quadrupole–quadrupole interactions, respectively. The $\frac{I_{s0}}{I_s} - C^{n/3}$ ($n = 6$, 8, 10) plots for the lanthanide-grafted TTA-DFP COF are shown in Figure S31. It can be seen that when $n = 6$, the $\frac{I_{s0}}{I_s}$ value follows the linear trend law better than for $n = 8$ or 10. This indicates that the dipole–dipole mechanism is the main way of energy transfer between Tb^{3+} and Eu^{3+} in this COF material.

CONCLUSIONS

To summarize, we have synthesized for the first time lanthanide-grafted COF materials (Ln@TTA-DFP COF) to obtain white-light emission. The excitation maximum of the as-synthesized TTA-DFP COF is around 370 nm, and the corresponding emission is at 439 nm (blue region) due to the inherent organic components of the COF. TTA-DFP COF was grafted with Eu^{3+} and Tb^{3+} complexes to yield the corresponding characteristic lanthanide emissions in the red and green regions when excited at 317 and 313 nm wavelengths, respectively. Furthermore, to obtain white-light emission, a mixture of Eu^{3+}/Tb^{3+} at appropriate ratios was grafted onto the COF. Exciting 10%Eu,90%Tb@TTA-DFP COF into the maximum of the excitation band resulted in orange emission, which could be converted to white-light emission by varying the excitation wavelength. When exciting

DOI: 10.1021/acsami.9b07779
ACS Appl. Mater. Interfaces 2019, 11, 27343–27352

at longer wavelengths, a blue component originated from the incomplete energy transfer from the organic ligand to Tb^{3+}, which allowed close to ideal white-light emission. A warm white light could also be obtained with 1%Eu,99%Tb@TTA-DFP COF by tuning the exciting wavelength.

As this is the first report of lanthanide COF materials, our results cannot be compared to other COF materials; however, it is interesting to note some similarities and dissimilarities between these Ln@TTA-DFP COF materials and other lanthanide-grafted porous materials. It seems that from the synthetic point of view, COFs are more difficult to graft with lanthanide ions than materials such as MOFs and zeolites of PMOs. For COFs, we have observed that to obtain a good loading of the Ln^{3+} ions in the COF and therefore strong luminescence properties, an excess of the lanthanide salt/complex should be used. On the other hand, MOFs can be successfully grafted with lanthanides employing equal molar amounts of the MOF.[24,54,55] PMOs can also be efficiently grafted without the use of excess lanthanide salts.[56] However, in some reports, an excess of the lanthanide salts is recommended.[57,29] Avoiding a preliminary soaking step has also been reported for other porous materials. The luminescence intensity and decay times of the Ln@TTA-DFP COF materials reported in this work can be well compared to other lanthanide-grafted porous materials. For example, the $Tb(hfac)_3$@TTA-DFP COF compound has a decay time of 951.3 μs, which can be well compared to other LnMOFs, LnPMOs, and lanthanide zeolites.[55,58−60] However, some lanthanide-grafted zeolites have been reported to have very long decay times.[61] In our mixed Eu,Tb materials, the calculated energy transfer from Tb to Eu is very high, up to 93.4%, for the 10%Eu,99%Tb@TTA-DFP COF material. Somewhat lower values are usually reported in Eu,Tb mixed MOF systems.[55,58,62] Energy transfer values have not been reported to date for similar Eu,Tb PMO materials. The quantum yields of our Ln@TTA-DFP COF materials are not very high, which is often the case also in LnMOF materials and lanthanide coordination polymers.[63] However, some LnMOFs with quite high quantum yields are also known in the literature.[55,64,65]

In this study, we introduce new hybrid materials through simple grafting of lanthanide complexes on 2D COFs for white-light luminescent applications. We have shown that this is a promising new class of materials that can be used as a support for grafting lanthanide ions and complexes for the purpose of obtaining white light as well as other luminescence applications. However, these materials still have some shortcomings such as a more challenging synthesis compared to similar MOFs or PMO material, but we believe this can be further optimized by varying the synthetic route. With this first report paving the road for Ln@COF synthesis, we expect many new exciting results will emerge soon.

■ ASSOCIATED CONTENT

Supporting Information

The Supporting Information is available free of charge on the ACS Publications website at DOI: 10.1021/acsami.9b07779.

Ligand synthetic procedures, FT-IR spectra, PXRD patterns, elemental analysis, pore size distributions, TGA, TEM-EDX, XPS, and luminescence results with decay times (PDF)

■ AUTHOR INFORMATION

Corresponding Authors

*E-mail: rik.vandeun@ugent.be (R.V.D.).
*E-mail: pascal.vandervoort@ugent.be (P.V.D.V.).

ORCID

Chidharth Krishnaraj: 0000-0001-8625-7322
Anna M. Kaczmarek: 0000-0001-5254-8762
Himanshu Sekhar Jena: 0000-0002-5869-5226
Rik Van Deun: 0000-0001-7091-6864
Pascal Van Der Voort: 0000-0002-4874-0943

Notes

The authors declare no competing financial interest.

■ ACKNOWLEDGMENTS

C.K. acknowledges the support from the Research Board of Ghent University (GOA010-17, BOF GOA2017000303). A.M.K. acknowledges Ghent University's Special Research Fund (BOF) for a Postdoctoral Mandate (project BOF15/PDO/091). H.S.J. acknowledges FWO [PEGASUS]2 Marie Sklodowska-Curie grant agreement no. 665501 for Incoming postdoctoral fellowship. The authors thank Prof. Vera Meynen and Dr. Karen Leyssens (University of Antwerp) for assisting with the porosity measurements. They also thank Katrien Haustraete for helping with the TEM measurements and Funda Aliiçc for helping with the elemental analysis.

■ REFERENCES

(1) Diercks, C. S.; Yaghi, O. M. The Atom, the Molecule, and the Covalent Organic Framework. *Science* **2017**, *355*, No. eaal1585.
(2) Zeng, Y.; Zou, R.; Zhao, Y. Covalent Organic Frameworks for CO_2 Capture. *Adv. Mater.* **2016**, *28*, 2855−2873.
(3) Zhi, Y.; Li, Z.; Feng, X.; Xia, H.; Zhang, Y.; Shi, Z.; Mu, Y.; Liu, X. Covalent Organic Frameworks as Metal-Free Heterogeneous Photocatalysts for Organic Transformations. *J. Mater. Chem. A* **2017**, *5*, 22933−22938.
(4) Lu, S.; Hu, Y.; Wan, S.; McCaffrey, R.; Jin, Y.; Gu, H.; Zhang, W. Synthesis of Ultrafine and Highly Dispersed Metal Nanoparticles Confined in a Thioether-Containing Covalent Organic Framework and their Catalytic Applications. *J. Am. Chem. Soc.* **2017**, *139*, 17082−17088.
(5) Wang, S.; Wang, Q.; Shao, P.; Han, Y.; Gao, X.; Ma, L.; Yuan, S.; Ma, X.; Zhou, J.; Feng, X.; Wang, B. Exfoliation of Covalent Organic Frameworks into Few-Layer Redox-Active Nanosheets as Cathode Materials for Lithium-Ion Batteries. *J. Am. Chem. Soc.* **2017**, *139*, 4258−4261.
(6) Du, Y.; Yang, H.; Whiteley, J. M.; Wan, S.; Jin, Y.; Lee, S. H.; Zhang, W. Ionic Covalent Organic Frameworks with Spiroborate Linkage. *Angew. Chem., Int. Ed.* **2016**, *55*, 1737−41.
(7) Mitra, S.; Sasmal, H. S.; Kundu, T.; Kandambeth, S.; Illath, K.; Díaz Díaz, D.; Banerjee, R. Targeted Drug Delivery in Covalent Organic Nanosheets (CONs) via Sequential Postsynthetic Modification. *J. Am. Chem. Soc.* **2017**, *139*, 4513−4520.
(8) Fang, Q.; Wang, J.; Gu, S.; Kaspar, R. B.; Zhuang, Z.; Zheng, J.; Guo, H.; Qiu, S.; Yan, Y. 3D Porous Crystalline Polyimide Covalent Organic Frameworks for Drug Delivery. *J. Am. Chem. Soc.* **2015**, *137*, 8352−8355.
(9) Das, S.; Heasman, P.; Ben, T.; Qiu, S. Porous Organic Materials: Strategic Design and Structure-Function Correlation. *Chem. Rev.* **2017**, *117*, 1515−1563.
(10) Feng, X.; Chen, L.; Honsho, Y.; Saengsawang, O.; Liu, L.; Wang, L.; Saeki, A.; Irle, S.; Seki, S.; Dong, Y.; Jiang, D. An Ambipolar Conducting Covalent Organic Framework with Self-Sorted and Periodic Electron Donor-Acceptor Ordering. *Adv. Mater.* **2012**, *24*, 3026−3031.

(11) Uribe-Romo, F. J.; Hunt, J. R.; Furukawa, H.; Klöck, C.; O'Keeffe, M.; Yaghi, O. M. A Crystalline Imine-Linked 3-D Porous Covalent Organic Framework. *J. Am. Chem. Soc.* **2009**, *131*, 4570−4571.
(12) Ding, S.-Y.; Cui, X.-H.; Feng, J.; Lu, G.; Wang, W. Facile Synthesis of −C═N− Linked Covalent Organic Frameworks under Ambient Conditions. *Chem. Commun.* **2017**, *53*, 11956−11959.
(13) Rogge, S. M. J.; Bavykina, A.; Hajek, J.; Garcia, H.; Olivos-Suarez, A. I.; Sepúlveda-Escribano, A.; Vimont, A.; Clet, G.; Bazin, P.; Kapteijn, F.; Daturi, M.; Ramos-Fernandez, E. V.; Llabrés I Xamens, F. X.; Van Speybroeck, V.; Gascon, J. Metal−Organic and Covalent Organic Frameworks as Single-Site Catalysts. *Chem. Soc. Rev.* **2017**, *46*, 3134−3184.
(14) Aiyappa, H. B.; Thote, J.; Shinde, D. B.; Banerjee, R.; Kurungot, S. Cobalt-Modified Covalent Organic Framework as a Robust Water Oxidation Electrocatalyst. *Chem. Mater.* **2016**, *28*, 4375−4379.
(15) Wan, S.; Guo, J.; Kim, J.; Ihee, H.; Jiang, D. A Belt-Shaped, Blue Luminescent, and Semiconducting Covalent Organic Framework. *Angew. Chem., Int. Ed.* **2008**, *47*, 8826−8830.
(16) Crowe, J. W.; Baldwin, L. A.; McGrier, P. L. Luminescent Covalent Organic Frameworks Containing a Homogeneous and Heterogeneous Distribution of Dehydrobenzoannulene Vertex Units. *J. Am. Chem. Soc.* **2016**, *138*, 10120−10123.
(17) Dalapati, S.; Jin, E.; Addicoat, M.; Heine, T.; Jiang, D. Highly Emissive Covalent Organic Frameworks. *J. Am. Chem. Soc.* **2016**, *138*, 5797−5800.
(18) Bessinger, D.; Ascherl, L.; Auras, F.; Bein, T. Spectrally Switchable Photodetection with Near-Infrared-Absorbing Covalent Organic Frameworks. *J. Am. Chem. Soc.* **2017**, *139*, 12035−12042.
(19) Li, X.; Gao, Q.; Wang, J.; Chen, Y.; Chen, Z.-H.; Xu, H.-S.; Tang, W.; Leng, K.; Ning, G.-H.; Wu, J.; Xu, Q.-H.; Quek, Y. S.; Lu, Y.; Loh, K. P. Tuneable Near White-Emissive Two-Dimensional Covalent Organic Frameworks. *Nat. Commun.* **2018**, *9*, No. 2335.
(20) Smith, T.; Guild, J. The C.I.E. Colorimetric Standards and their Use. *Trans. Opt. Soc.* **1932**, *33*, 73−134.
(21) Haldar, S.; Chakraborty, D.; Roy, B.; Banappanavar, G.; Rinku, K.; Mullangi, D.; Hazra, P.; Kabra, D.; Vaidhyanathan, R. Anthracene-Resorcinol Derived Covalent Organic Framework as Flexible White Light Emitter. *J. Am. Chem. Soc.* **2018**, *140*, 13367−13374.
(22) Ding, H.; Li, J.; Xie, G.; Lin, G.; Chen, R.; Peng, Z.; Yang, C.; Wang, B.; Sun, J.; Wang, C. An AIEgen-Based 3D Covalent Organic Framework for White Light-Emitting Diodes. *Nat. Commun.* **2018**, *9*, No. 5234.
(23) De Almeida, A.; Santos, B.; Paolo, B.; Quicheron, M. Solid State Lighting Review - Potential and Challenges in Europe. *Renewable Sustainable Energy Rev.* **2014**, *34*, 30−48.
(24) Bender, V. C.; Marchesan, T. B.; Alonso, J. M. Solid-State Lighting: A Concise Review of the State of the Art on LED and OLED Modeling. *IEEE Ind. Electron. Mag.* **2015**, *9*, 6−16.
(25) Branas, C.; Azcondo, F. J.; Alonso, J. M. Solid-State Lighting: A System Review. *IEEE Ind. Electron. Mag.* **2013**, *7*, 6−14.
(26) Zhao, Y.; Guo, L.; Gándara, F.; Ma, Y.; Liu, Z.; Zhu, C.; Lyu, H.; Trickett, A. C.; Kapustin, A. E.; Terasaki, O.; Yaghi, M. O. A Synthetic Route for Crystals of Woven Structures, Uniform Nanocrystals, and Thin Films of Imine Covalent Organic Frameworks. *J. Am. Chem. Soc.* **2017**, *139*, 13166−13172.
(27) Martinez-Gomez, N. C.; Vu, H. N.; Skovran, E. Lanthanide Chemistry: From Coordination in Chemical Complexes Shaping Our Technology to Coordination in Enzymes Shaping Bacterial Metabolism. *Inorg. Chem.* **2016**, *55*, 10083−10089.
(28) Kaczmarek, A. M.; Liu, Y. Y.; Wang, C.; Laforce, B.; Vincze, L.; Van Der Voort, P.; Van Hecke, K.; Van Deun, R. Lanthanide "Chameleon" Multistage Anti-Counterfeit Materials. *Adv. Funct. Mater.* **2017**, *27*, No. 1700258.
(29) Kaczmarek, A. M.; Esquivel, D.; Ouwehand, J.; Van Der Voort, P.; Romero-Salguero, F. J.; Van Deun, R. Temperature Dependent NIR Emitting Lanthanide-PMO/Silica Hybrid Materials. *Dalton Trans.* **2017**, *46*, 7878−7887.
(30) Esquivel, D.; Kaczmarek, A. M.; Jiménez-Sanchidrián, C.; Van Deun, R.; Romero-Salguero, F. J.; Van Der Voort, P. Eu^{3+}@PMO: Synthesis, Characterization and Luminescence Properties. *J. Mater. Chem. C* **2015**, *3*, 2909−2917.
(31) Decadt, R.; Van Hecke, K.; Depla, D.; Leus, K.; Weinberger, D.; Van Driessche, I.; Van Der Voort, P.; Van Deun, R. Synthesis, Crystal Structures, and Luminescence Properties of Carboxylate Based Rare-Earth Coordination Polymers. *Inorg. Chem.* **2012**, *51*, 11623−11634.
(32) Yang, X.; Lin, X.; Zhao, Y.; Zhao, Y. S.; Yan, D. Lanthanide Metal−Organic Framework Microrods: Colored Optical Waveguides and Chiral Polarized Emission. *Angew. Chem., Int. Ed.* **2017**, *56*, 7853−7857.
(33) Wang, Y.; Li, H. Luminescent Materials of Zeolite Functionalized with Lanthanides. *CrystEngComm* **2014**, *16*, 9764−9778.
(34) Wang, Y.; Li, H.; Gu, L.; Gan, Q.; Li, Y.; Calzaferri, G. Thermally Stable Luminescent Lanthanide Complexes in Zeolite L. *Microporous Mesoporous Mater.* **2009**, *121*, 1−6.
(35) Roberts, R. J.; Le, D.; Leznoff, D. B. Color-Tunable and White-Light Luminescence in Lanthanide−Dicyanoaurate Coordination Polymers. *Inorg. Chem.* **2017**, *56*, 7948−7959.
(36) Li, S.-M.; Zheng, X.-J.; Yuan, D.-Q.; Ablet, A.; Jin, L.-P. In Situ Formed White-Light-Emitting Lanthanide−Zinc−Organic Frameworks. *Inorg. Chem.* **2012**, *51*, 1201−1203.
(37) Shavaleev, N. M.; Eliseeva, S. V.; Scopelliti, R.; Bünzli, J. C. G. Tridentate Benzimidazole-Pyridine-Tetrazolates as Sensitizers of Europium Luminescence. *Inorg. Chem.* **2014**, *53*, 5171−5178.
(38) Shavaleev, N. M.; Eliseeva, S. V.; Scopelliti, R.; Bünzli, J. C. G. Designing Simple Tridentate Ligands for Highly Luminescent Europium Complexes. *Chem. Eur. J.* **2009**, *15*, 10790−10802.
(39) Binnemans, K. Interpretation of Europium(III) Spectra. *Coord. Chem. Rev.* **2015**, *295*, 1−45.
(40) Binnemans, K. Rare-Earth Beta-Diketonates. In *Handbook on the Physics and Chemistry of Rare Earths*; North Holland, 2005; Vol. *35*, pp 107−272.
(41) Ding, S.-Y.; Gao, J.; Wang, Q.; Zhang, Y.; Song, W.-G.; Su, C.-Y.; Wang, W. Construction of Covalent Organic Framework for Catalysis: Pd/COF-LZU1 in Suzuki-Miyaura Coupling Reaction. *J. Am. Chem. Soc.* **2011**, *133*, 19816−19822.
(42) Das, G.; Benyettou, F.; Sharama, S. K.; Prakasam, T.; Gándara, F.; de la Peña-O'Shea, V. A.; Saleh, N.; Pasricha, R.; Jagannathan, R.; Olson, M. A.; Trabolsi, A. Covalent Organic Nanosheets for Bioimaging. *Chem. Sci.* **2018**, *9*, 8382−8387.
(43) Li, Z.; Li, H.; Guan, X.; Tang, J.; Yusran, Y.; Li, Z.; Xue, M.; Fang, Q.; Yan, Y.; Valtchey, V.; Qiu, S. Three-Dimensional Ionic Covalent Organic Frameworks for Rapid, Reversible, and Selective Ion Exchange. *J. Am. Chem. Soc.* **2017**, *139*, 17771−17774.
(44) Hu, Y.; Goodeal, N.; Chen, Y.; Ganose, A. M.; Palgrave, R. G.; Bronstein, H.; Blunt, M. O. Probing the Chemical Structure of Monolayer Covalent-Organic Frameworks Grown via Schiff-base Condensation Reactions. *Chem. Commun.* **2016**, *52*, 9941−9944.
(45) Li, X.; Zhang, C.; Cai, S.; Lei, X.; Altoe, V.; Hong, F.; Urban, J. J.; Ciston, J.; Chan, E. M.; Liu, Y. Facile Transformation of Imine Covalent Organic Frameworks into Ultrastable Crystalline Porous Aromatic Frameworks. *Nat. Commun.* **2018**, *9*, No. 2998.
(46) Mercier, F.; Alliot, C.; Bion, L.; Thromat, N.; Toulhoat, P. XPS Study of Eu(III) Coordination Compounds: Core Levels Binding Energies in Solid Mixed-oxo-compounds $Eu_mX_xO_y$. *J. Electron Spectrosc. Relat. Phenom.* **2006**, *150*, 21−26.
(47) Vercaemst, R.; Poelman, D.; Van Meirhaegehe, R. L.; Fiermans, L.; Laflère, W. H.; Cardon, F. An XPS Study of the Dopants' Valence States and the Composition of $CaS_{1-x}Se_x$: Eu and $SrS_{1-x}Se_x$: Ce Thin Film Electroluminescent Devices. *J. Lumin.* **1995**, *63*, 19−30.
(48) Swart, H. C.; Nagpure, I. M.; Ntwaeaborwa, O. M.; Fisher, G. L.; Terblans, J. J. Identification of Eu Oxidation States in a Doped Sr5(PO4)3F Phosphor by TOF-SIMS Imaging. *Opt. Express* **2012**, *20*, 17119−17125.

DOI: 10.1021/acsami.9b07779
ACS Appl. Mater. Interfaces 2019, 11, 27343−27352

(49) Pemba-Mabiala, J. M.; Lenzi, M.; Lenzi, J.; Lebugle, A. XPS Study of Mixed Cerium-Terbium Orthophosphate Catalysts. *Surf. Interface Anal.* **1990**, *15*, 663−667.
(50) Kalkowski, G.; Kaindl, G.; Wortmann, G.; et al. 4f-ligand Hybridization in CeF4 and TbF4 Probed by Core-level Spectroscopies. *Phys. Rev. B* **1988**, *37*, 1376−1382.
(51) Baur, F.; Glocker, F.; Jüstel, T. Photoluminescence and Energy Transfer Rates and Efficiencies in Eu3+ Activated Tb2Mo3O12. *J. Mater. Chem. C* **2015**, *3*, 2054−2064.
(52) Luo, Y.; Liu, Z.; Wong, H. T.; Zhou, L.; Wong, K.-L.; Shiu, K. K.; Tanner, P. A. Energy Transfer between Tb3+ and Eu3+ in LaPO4: Pulsed versus Switched-off Continuous Wave Excitation. *Adv. Sci.* **2019**, *6*, No. 1970060.
(53) Wang, B.; Ren, Q.; Hai, O.; Wu, X. Luminescence Properties and Energy Transfer in Tb3+ and Eu3+ Co-doped Ba2P2O7 Phosphors. *RSC Adv.* **2017**, *7*, 15222−15227.
(54) Kaczmarek, A. M.; Liu, Y.-Y.; Wang, C.; Laforce, B.; Vincze, L.; Van Der Voort, P.; Van Deun, R. Grafting of a Eu3+-tfac Complex on to a Tb3+-Metal Organic Framework for Use as a Ratiometric Thermometer. *Dalton Trans.* **2017**, *46*, 12717−12723.
(55) Zhou, Y.; Yan, B.; Lei, F. Postsynthetic Lanthanide Functionalization of Nanosized Metal−Organic Frameworks for Highly Sensitive Ratiometric Luminescent Thermometry. *Chem. Commun.* **2014**, *50*, 15235−15238.
(56) Li, Y.; Yan, B.; Li, Y.-J. Sulfide Functionalized Lanthanide (Eu/Tb) Periodic Mesoporous Organosilicas (PMOs) Hybrids with Covalent Bond: Physical Characterization and Photoluminescence. *Microporous Mesoporous Mater.* **2010**, *132*, 87−93.
(57) Guo, X.; Guo, H.; Fu, L.; Zhang, H.; Deng, R.; Sun, L.; Feng, J.; Dang, S. Novel Hybrid Periodic Mesoporous Organosilica Material Grafting with Tb Complex: Synthesis, Characterization and Photoluminescence Property. *Microporous Mesoporous Mater.* **2009**, *119*, 252−258.
(58) Zhang, H.; Shan, X.; Ma, Z.; Zhou, L.; Zhang, M.; Lin, P.; Hu, S.; Ma, E.; Li, R.; Du, S. A Highly Luminescent Chameleon: Fine-Tuned Emission Trajectory and Controllable Energy Transfer. *J. Mater. Chem. C* **2014**, *2*, 1367−1371.
(59) Liu, Y.-Y.; Decadt, R.; Bogaers, T.; Hemelsoet, K.; Kaczmarek, A. M.; Poelman, D.; Waroquier, M.; Van Speybroeck, V.; Van Deun, R.; Van Der Voort, P. Bipyridine-Based Nanosized Metal−Organic Framework with Tunable Luminescence by a Postmodification with Eu(III): An Experimental and Theoretical Study. *J. Phys. Chem. C* **2013**, *117*, 11302−11310.
(60) Kaczmarek, A. M.; Van Der Voort, P. Chemical Sensors based on Nano-Sized Lanthanide-Grafted Periodic Mesoporous Organosilica Hybrid Materials. *J. Mater. Chem. C* **2019**, 8109−8119.
(61) Wang, Y.; Li, H.; Zhang, W.; Liu, B. Luminescence Properties of Nanozeolite L Grafted with Terbium Organic Complex. *Mater. Lett.* **2008**, *62*, 3167−3170.
(62) Cui, Y.; Xu, H.; Yue, Y.; Guo, Z.; Yu, J.; Chen, Z.; Gao, J.; Yang, Y.; Qian, G.; Chen, B. A Luminescent Mixed-Lanthanide Metal−Organic Framework Thermometer. *J. Am. Chem. Soc.* **2012**, *134*, 3979−3982.
(63) Kaczmarek, A. M. Eu3+/Tb3+ and Dy3+ POM@MOFs and 2D Coordination Polymers based on Pyridine-2,6-dicarboxylic Acid for Ratiometric Optical Temperature Sensing. *J. Mater. Chem. C* **2018**, *6*, 5916−5925.
(64) Zhang, H.; Shan, X.; Ma, Z.; Zhou, L.; Zhang, M.; Lin, P.; Hu, S.; Ma, E.; Li, R.; Du, S. A Highly Luminescent Chameleon: Fine-Tuned Emission Trajectory and Controllable Energy transfer. *J. Mater. Chem. C* **2014**, *2*, 1367−1371.
(65) Zhu, M.; Hao, Z.-M.; Song, X.-Z.; Meng, X.; Zhao, S.-N.; Song, S-Y.; Zhang, H.-J. A New Type of Double-Chain based 3D Lanthanide(III) Metal−Organic Framework Demonstrating Proton Conduction and Tunable Emission. *Chem. Commun.* **2014**, *50*, 1912−1914.

DOI: 10.1021/acsami.9b07779
ACS Appl. Mater. Interfaces 2019, 11, 27343−27352